Chinese Chemical Letters 34 (2023) 107232

Contents lists available at ScienceDirect

Chinese Chemical Letters

journal homepage: www.elsevier.com/locate/cclet

Nitrogen doped hollow carbon nanospheres as efficient polysulfide restricted layer on commercial separators for high-performance lithium-sulfur batteries

Yue Zhao[a,b,1], Zhi Gu[b,c,1], Wei Weng[b,d], Dan Zhou[e], Ziqiang Liu[b,d], Wentong Fan[b], Shungui Deng[b], Hao He[a,*], Xiayin Yao[b,d,*]

[a] Key Laboratory of Material Physics, Ministry of Education, School of Physics and Microelectronics, Zhengzhou University, Zhengzhou 450001, China
[b] Ningbo Institute of Materials Technology and Engineering, Chinese Academy of Sciences, Ningbo 315201, China
[c] Department of Chemical and Environmental Engineering, Faculty of Science and Engineering, University of Nottingham, Ningbo 315100, China
[d] Center of Materials Science and Optoelectronics Engineering, University of Chinese Academy of Sciences, Beijing 100049, China
[e] Chongqing Key Laboratory of Extraordinary Bond Engineering and Advanced Materials Technology, College of Materials Science and Engineering, Yangtze Normal University, Chongqing 408100, China

ARTICLE INFO

Article history:
Received 12 January 2022
Revised 6 February 2022
Accepted 15 February 2022
Available online 19 February 2022

Keywords:
Nitrogen doped hollow carbon nanospheres
Separator modification
Shuffle effect
Polysulfides
Lithium-sulfur batteries

ABSTRACT

The polysulfide shuttle limits the development of lithium-sulfur (Li-S) batteries with high energy density and long lifespan. Herein, nitrogen doped hollow carbon nanospheres (NHCS) derived from polymerization of dopamine on SiO_2 nanospheres are employed to modify the commercial polypropylene/polyethylene/polypropylene tri-layer separators (PP/PE/PP@NHCS). The abundant nitrogen heteroatoms in NHCS exhibit strong chemical adsorption toward polysulfides, which can effectively suppress the lithium polysulfides shuttle and further enhance the utilization of active sulfur. Lithium-sulfur batteries employing the PP/PE/PP@NHCS deliver an initial discharge capacity of 1355 mAh/g and retain high capacity of 921 mAh/g after 100 cycles at 0.2 C. At a high rate of 2 C, the lithium-sulfur batteries exhibit capacity of 461 mAh/g after 1000 cycles with a capacity fading rate of 0.049% per cycle. This work demonstrates that the NHCS coated PP/PE/PP separator is promising for future commercial applications of lithium-sulfur batteries with improved electrochemical performances.

Lithium-sulfur batteries are considered as promising next generation rechargeable batteries owing to the high theoretical specific capacity of 1675 mAh/g and low cost, natural abundance as well as environmentally-friendliness of sulfur [1–3]. However, the practical applications of Li-S batteries have been hindered by several challenges, such as the insulating property of sulfur, large volumetric variation, lithium metal corrosion and shuttle effect caused by dissolution and migration of higher-order lithium polysulfides (Li_2S_x, $4 \leq x \leq 8$), which lead to irreversible capacity loss and limited cycle lifespan [4,5].

To address these problems, various strategies such as optimization of cathode materials [6,7], well design of functional electrolytes [8–10] and functionalization of separator [11–13] have been developed. The commercial Li-S battery separators with electrical insulating property and porous pathways play a key role in maintaining lithium ion transport and hindering internal short circuit. However, the shuttle effect of higher-order lithium polysulfides through separators inevitably results in the active materials loss and severe side reactions [14,15]. Rational separator modification was supposed to overcome mentioned challenges of Li-S batteries [13,16]. Recently, various carbon-based materials such as carbon nanotubes [17], carbon spheres [18] and graphene [19] have been used to modify separators owing to their excellent electrical conductivity, high specific surface area, good porosity and easy preparation. The carbon-decorated separators can effectively inhibit the migration of polysulfides and provide an extended conductive network on the cathode side, which promote the utilization of sulfur and suppress internal resistance of Li-S batteries [20]. However, these nonpolar carbon-based materials could only restrict the shuffle effect weakly by the faint physical affinity [21,22].

Doping of heteroatoms, such as N and O, in carbon materials is a convenient and effective method to realize chemical adsorption of polysulfides. The introduction of N atoms in carbon materials can provide lone pair electrons, so that polysulfides can be an-

* Corresponding authors.
E-mail addresses: hehao@zzu.edu.cn (H. He), yaoxy@nimte.ac.cn (X. Yao).
[1] These authors contributed equally to this work.

https://doi.org/10.1016/j.cclet.2022.02.037
1001-8417/

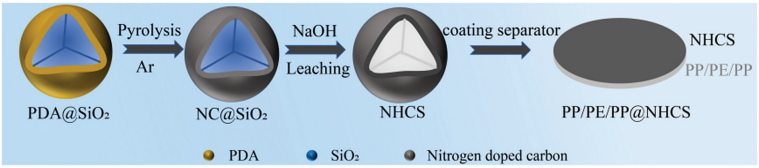

Fig. 1. Schematic diagram of the synthesis process of PP/PE/PP@NHCS separator.

chored by dipole-dipole electrostatic interaction between carbon-based materials and polysulfides during charge and discharge process [7,23]. Therefore, it is important to introduce a simple method to prepare carbon materials with homogeneous distribution of heteroatoms. Dopamine with rich amino groups can self-polymerize on the surface of various materials through one-step preparation in alkaline environment, which can further form carbon material precursors with various morphologies and uniform distribution of nitrogen and oxygen [24–26].

In this work, an effective separator modification strategy was proposed. Through template-assisted and pyrolysis methods, nitrogen doped hollow carbon spheres (NHCS) were prepared. The NHCS coated on the PP/PE/PP separators (PP/PE/PP@NHCS) not only acts as a secondary current collector to promote the migration of lithium ions and reinforce sulfur reutilization [17,19], but also can physically block and chemically adsorb lithium polysulfides. Meanwhile, large specific surface area, high porosity and rich nitrogen elements of NHCS can provide persistent electron transfer channels and a large number of active sites to facilitate a fast sulfur redox reaction and to reduce the volume expansion of cathode during charge-discharge process. Lithium-sulfur batteries employing the PP/PE/PP@NHCS separator exhibit high capacity and stable cyclic performance.

The procedure for the preparation of the PP/PE/PP@NHCS was illustrated in Fig. 1. Dopamine was firstly self-polymerized on the SiO_2 nanosphere template in alkaline environment. After pyrolysis process under Ar atmosphere, the obtained nitrogen doped carbon coated SiO_2 ($NC@SiO_2$) was then rinsed in 4 mol/L NaOH solution to remove the SiO_2 template and finally acquire the nitrogen doped hollow carbon spheres (NHCS). Subsequently, the PP/PE/PP@NHCS separators were prepared by a facile blade-coating approach and its optical picture of the PP/PE/PP@NHCS separator can be found in Fig. S1 (Supporting information). As shown in Fig. 2a, the broad diffraction peak at around 23° for NHCS indicates its amorphous nature, which is similar to nitrogen doped carbon (NC) (Fig. S2 in Supporting information). Graphitization degree of NC and NHCS were characterized by Raman test. The intensities of D-band (1347 cm^{-1}) to G-band (1586 cm^{-1}) are 0.918 and 0.948 for NC and NHCS respectively, indicating the lower degree of graphitization of the NHCS (Fig. 2b). The pore size distribution and the specific surface area were further characterized by nitrogen adsorption–desorption isothermal measurements. Compared with the BET specific surface area of 441 m^2/g for NC, NHCS exhibits much larger BET specific surface area of 490 m^2/g (Table S1 in Supporting information and Fig. 2c). In addition, the adsorption and desorption isotherm of NHCS shows a typical IV isotherm, which is a characteristic of mesoporous materials. It can be seen from Fig. S3 (Supporting information) that the formation of mesopores in NHCS centered at around 4 nm may be caused by hollow nanosphere structure and the release of volatiles during the annealing procession, while the pore size of about 53 nm may be corresponding to the loose interspaces of NHCS and macropores produced after elimination of silica template [27,28]. The abundant mesopores, large specific surface and the hollow structure of NHCS can provide vast reaction active sites, enhancing the adsorption of polysulfides and suppressing the loss of active materials. As

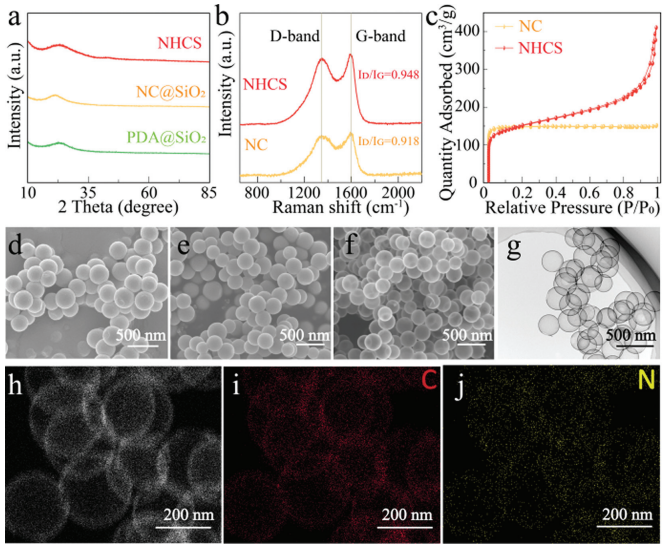

Fig. 2. (a) XRD patterns of $PDA@SiO_2$, $NC@SiO_2$ and NHCS. (b) Raman spectra of NC and NHCS. (c) N_2 adsorption and desorption isotherms of NC and NHCS. SEM images of (d) $PDA@SiO_2$, (e) $NC@SiO_2$ and (f) NHCS. (g) TEM image and (h-j) EDS mapping of NHCS.

shown in Figs. 2d-f, $PDA@SiO_2$, $NC@SiO_2$ and NHCS exhibit similar spherical shape with a diameter of around 300 nm, while NC shows irregular and stacked morphology with a diameter of about 2 μm (Fig. S4 in Supporting information). TEM images of NHCS reveal the hollow spherical structure (Fig. 2g) and the EDS element mapping demonstrates uniform distribution of N elements along carbon shell (Figs. 2h-j). The thickness of the NHCS layer is determined around 11 μm as presented in Fig. S5 (Supporting information). The mass loading of NHCS layer (about 0.13 mg/cm^2) is much lower than those of modified separators reported in the previous works (Table S2 in Supporting information) [4,29-33].

CR2032 coin cells using the S/C electrodes, PP/PE/PP or PP/PE/PP@NHCS separators and lithium anode were assembled to estimate their electrochemical performances. Fig. 3a presents the CV curves of the first-three cycles of PP/PE/PP-assembled Li-S batteries at a sweep rate of 0.1 mV/s. During the first cathodic scan, two pronounced peaks at 2.23 and 1.93 V correspond to the reduction of S_8 to high-order polysulfides and further conversion to Li_2S_2/Li_2S, respectively [34]. During the first anodic scan, two tight peaks at 2.34 and 2.41 V correspond to the oxidation of Li_2S_2/LiS_2 to S_8 [7]. As shown in Fig. 3b, the PP/PE/PP@NHCS-assembled Li-S batteries display higher current intensities and the narrower potential hysteresis ($\Delta E = 0.13$ V) between cathodic peak (R1) and anodic peak (O1) at first scan than those of the PP/PE/PP-assembled Li-S batteries ($\Delta E = 0.18$ V), demonstrating its smaller electrochemical polarization and faster reaction kinetics [32,33]. During the following cycles, the CV curves of PP/PE/PP@NHCS-assembled Li-S batteries exhibit good consistency and stability, indicating its excellent electrochemical reversibility and ability to restrict polysulfides dissolution [7]. The CV curves of PP/PE/PP and PP/PE/PP@NHCS-

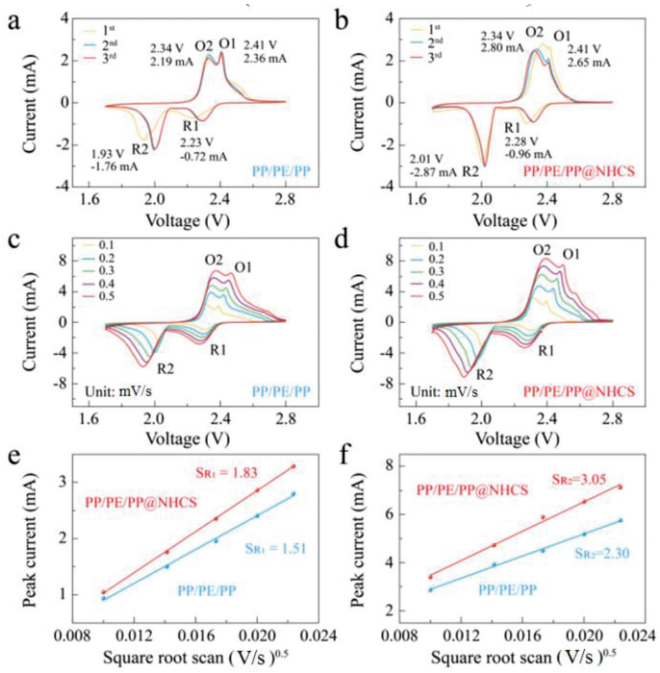

Fig. 3. CV profiles of Li-S batteries employing the (a) PP/PE/PP and (b) PP/PE/PP@NHCS separators at 0.1 mV/s. CV profiles of Li-S batteries employing the (c) PP/PE/PP and (d) PP/PE/PP@NHCS at different scan rates. Liner fit of the peak currents *versus* the square root of scan rates corresponding to (e) the first cathodic process and (f) the second cathodic process for the PP/PE/PP and PP/PE/PP@NHCS-assembled Li-S batteries.

assembled Li-S batteries at various scan rates from 0.1 mV/s to 0.5 mV/s are shown in Figs. 3c and d. The peak current densities display a linear relationship related to the square root of scanning rates, and the fitting slope values show proportional relationship with the lithium ionic diffusion coefficient by classical Randles-Sevick equation [35,36]. According to the fitting results (Figs. 3e and f, Fig. S6 in Supporting information), PP/PE/PP@NHCS-assembled Li-S batteries display higher peak current densities and slopes ($S_{R1} = 1.83$ and $S_{R2} = 3.05$, $S_{O1} = 3.84$ and $S_{O2} = 4.19$) than these of PP/PE/PP-assembled Li-S batteries ($S_{R1} = 1.51$ and $S_{R2} = 2.30$, $S_{O1} = 3.39$ and $S_{O2} = 3.45$), showing its faster ion diffusion [26].

Furthermore, the ionic conductivities of PP/PE/PP and PP/PE/PP@NHCS separators were tested by using EIS measurements in symmetric cells, as shown in Fig. S7 (Supporting information). Limited by low porosity and lithium ionic insulation, commercial PP/PE/PP separator shows low ionic conductivity of 0.205 mS/cm. In contrast, PP/PE/PP@NHCS separator displays a high ionic conductivity (0.627 mS/cm), which could be ascribed to the abundant mesopores, the existence of N atoms and interconnected conductive network of NHCS coating layer.

To further characterize the electrocatalytic activity of NHCS coating layer to the polysulfide redox reactions, CV tests were conducted using PP/PE/PP@NHCS separators and 0.2 mol/L Li_2S_6 electrolyte at a scan rate of 2 mV/s between −1 V and 1 V. As shown in Fig. 4a, two distinct peaks at −0.069 (peak I) and −0.523 V (peak II) are corresponding to the reduction of Li_2S_6 to short-chain lithium polysulfides and further conversion to Li_2S/Li_2S_2, respectively. The peaks at 0.028 (peak III) and 0.187 (peak IV) were attributed to the oxidation of Li_2S/Li_2S_2 to L_2S_6 and Li_2S_6 to the final sulfur element, respectively [37]. Compared to the PP/PE/PP separators, the symmetric batteries with the PP/PE/PP@NHCS separators display higher current intensity and narrower gap between the two peaks, indicating rapid polysulfide redox conversion reactions

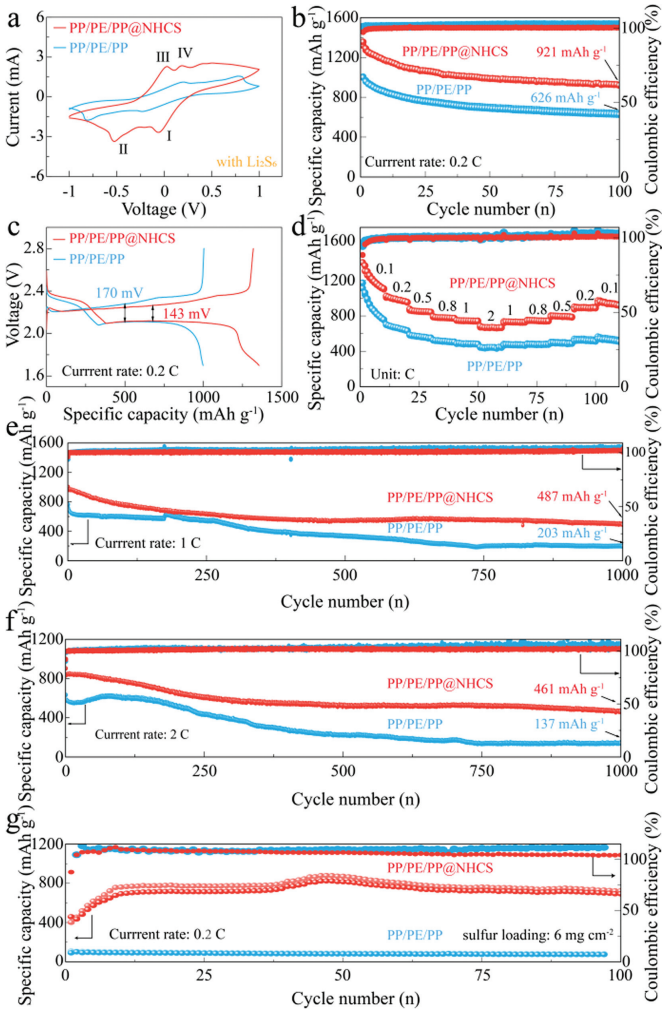

Fig. 4. (a) CV curves of symmetric cell with 0.2 mol/L Li_2S_6 of PP/PE/PP and PP/PE/PP@NHCS separator at scan rate of 2 mV/s. (b) Cyclic performance and (c) charge-discharge plots of the Li-S batteries with PP/PE/PP and PP/PE/PP@NHCS separators at 0.2 C. Cyclic performance of the Li-S batteries with PP/PE/PP and PP/PE/PP@NHCS separator at (d) varied rates, (e) 1 C and (f) 2 C. (g) Cyclic performance of the Li-S batteries with PP/PE/PP and PP/PE/PP@NHCS separator at 0.2 C under high sulfur loading of 6 mg/cm^2.

enhanced by NHCS coating layer. Meanwhile, no current response was observed for PP/PE/PP@NHCS separator based the symmetric batteries without Li_2S_6, confirming that the current response is caused by the redox reaction of Li_2S_6 and NHCS coating layer does not provide the capacity contribution in Li-S batteries (Fig. S8 in Supporting information) [32,38].

The cyclic performances of Li-S batteries at 0.2 C are displayed in Fig. 4b. For PP/PE/PP-assembled Li-S battery, it delivers an initial discharge capacity of 999 mAh/g and retains at 626 mAh/g after 100 cycles. By contrast, the PP/PE/PP@NHCS-assembled Li-S battery shows an initial discharge capacity of 1355 mAh/g and a high capacity of 921 mAh/g after 100 cycles, benefiting from the high utilization of sulfur from the enhanced ionic conductivity of PP/PE/PP@NHCS separators. The corresponding galvanostatic charge/discharge profiles of PP/PE/PP and PP/PE/PP@NHCS assembled Li-S batteries at 0.2 C are shown in Fig. 4c. Each curve shows one charge plateau and two discharge plateaus, corresponding to the oxidation of Li_2S_2/Li_2S to S_8 and reduction of S_8 to long-chain lithium polysulfides then to Li_2S_2/Li_2S, respectively, which is consistent with the CV results of Li-S batteries (Figs. 3a and b). The voltage hysteresis between charge and discharge are 170 and

143 mV for PP/PE/PP-assembled and PP/PE/PP@NHCS-assembled Li-S batteries, respectively, demonstrating the smaller overpotential for PP/PE/PP@NHCS-based configuration. The rate performances and corresponding charge and discharge voltage curves of the Li-S batteries using PP/PE/PP and PP/PE/PP@NHCS separators are shown in Fig. 4d and Fig. S9 (Supporting information). PP/PE/PP@NHCS-assembled Li-S batteries show discharge specific capacities of 1585, 1023, 877, 793, 750, 684 mAh/g at 0.1, 0.2, 0.5, 0.8, 1 and 2 C, respectively, showing higher specific capacities than those of PP/PE/PP-assembled Li-S batteries at corresponding C-rates. And when current density returns from 2 C to 0.1 C, the discharge specific capacity for PP/PE/PP@NHCS-assembled Li-S batteries recovers to 943.7 mAh/g, which is higher than the PP/PE/PP-assembled Li-S batteries of 511 mAh/g, demonstrating an excellent rate reversibility. The long cyclic performances of Li-S batteries using PP/PE/PP and PP/PE/PP@NHCS separators were further investigated (Figs. 4e and f). The PP/PE/PP@NHCS-assembled Li-S batteries deliver excellent cycling stability with high initial discharge capacities of 1002 and 903 mAh/g. And the discharge capacities maintain at 487 and 461 mAh/g with low capacity fading rates of 0.051% and 0.049% per cycle after 1000 cycles at 1 and 2 C, respectively, which is superior to previously reported functional separators (Table S2 in Supporting information). In comparison, the PP/PE/PP-assembled Li-S batteries display inferior cycling stability with discharge capacities of 763 and 633 mAh/g, retaining discharge capacities of 203 and 137 mAh/g and fading rates of 0.073% and 0.078% per cycle after 1000 cycles at 1 and 2 C, respectively. Meanwhile, the corresponding discharge-charge profiles are displayed in Fig. S10 (Supporting information), demonstrating the longer plateau, smaller potential polarization and improved conversion reversibility of PP/PE/PP@NHCS assembled Li-S batteries. Even at a high sulfur loading of 6 mg/cm^2, PP/PE/PP@NHCS-assembled Li-S batteries still exhibit good cycle stability with a capacity of 692 mAh/g at 0.2 C for 100 cycles (Fig. 4g). The enhanced capacities, reduced polarization and accelerated polysulfide redox reaction kinetics can be ascribed to the adsorption of polysulfides by heteroatoms, the physical barrier and the extended conductive network from the NHCS.

The EIS measurements of Li-S batteries with the PP/PE/PP (Fig. S11a in Supporting information) and PP/PE/PP@NHCS (Fig. S11b in Supporting information) separators before and after 10, 20, 50 and 100 cycles at 1 C were performed to testify the reaction kinetics with the PP/PE/PP@NHCS separators. PP/PE/PP@NHCS-assembled Li-S batteries exhibit smaller charge transfer impedance and ion diffusion resistance than those of PP/PE/PP-assembled Li-S batteries, which ascribes from the high electrical conductivity of NHCS, improved interfacial affinity between NHCS and polysulfides and quicker charge transport. After 10 cycles, the dramatic reduction of resistance is due to the activation process of electrode materials. The smaller change of EIS curves for PP/PE/PP@NHCS-assembled Li-S batteries than that of PP/PE/PP-assembled Li-S batteries during cycling indicates highly reversible redox conversion and excellent stability from PP/PE/PP@NHCS separator. After 100 cycles, the hollow morphologies were well retained without obvious transformation (Fig. S12 in Supporting information). To further investigate the ability of restricting polysulfide shuttle, the cross-section sulfur element mapping for PP/PE/PP and PP/PE/PP@NHCS separators after cycling at 1 C were measured (Fig. S13 in Supporting information). Compared with the concentrated distribution of S element across the pure separator layer, large amounts of S element were confined in the NHCS layer coated on one side of PP/PE/PP separator, indicating that NHCS coating layer could well hinder the movement of polysulfides. The suppress of polysulfides shuttle can also be confirmed by the polysulfides permeation experiment on PP/PE/PP and PP/PE/PP@NHCS separator (Fig. S14 in Supporting information). When fixing the solution without polysulfides on the right side of H-type cell, the solution quickly turned deep yellow after 3 h. On the contrary, for the PP/PE/PP@NHCS separator, the transparent solution changed to light yellow after 5 h, confirming the restricted shuttling effects by the introduction of the NHCS coating layer for the PP/PE/PP separator.

In summary, PP/PE/PP@NHCS separator was developed to enhance the electrochemical performance of lithium-sulfur batteries. The unique hollow spherical morphology, and abundant nitrogen heteroatoms can reduce the unexpected shuttling effects of polysulfide. Meanwhile, PP/PE/PP@NHCS displays excellent ion diffusion and fast reaction kinetics owing to its large specific surface area, high porosity and extended conductive network. The Li-S batteries based on PP/PE/PP@NHCS separator deliver excellent cycling stability and a high discharge capacity of 461 mAh/g after 1000 cycles at 2 C with a low capacity fading rate of 0.049% per cycle.

Declaration of competing interest

The authors declare that they have no known competing financial interests or personal relationships that could have appeared to influence the work reported in this paper.

Acknowledgments

The work was supported by the National Natural Science Foundation of China (Nos. U1964205, 51872303, 52172253), Zhejiang Provincial Natural Science Foundation of China (No. LD18E020004), Ningbo S&T Innovation 2025 Major Special Programme (Nos. 2019B10044, 20211ZDYF020077), Zhejiang Provincial Key R&D Program of China (No. 2022C01072), Chongqing Research Program of Basic Research and Frontier Technology (No. cstc2019jcyj-msxmX0510) and Youth Innovation Promotion Association CAS (No. 2017342).

Supplementary materials

Supplementary material associated with this article can be found, in the online version, at doi:10.1016/j.cclet.2022.02.037.

References

[1] D.W. Su, D. Zhou, C.Y. Wang, G.X. Wang, Adv. Funct. Mater. 28 (2018) 1800154.
[2] S.F. Jiang, S. Huang, M.J. Yao, et al., Chin. Chem. Lett. 31 (2020) 2347–2352.
[3] M.M. Thackeray, C. Wolverton, E.D. Isaacs, Energy Environ. Sci. 5 (2012) 7854–7863.
[4] X.L. Wang, G.R. Li, M.J. Li, et al., J. Energy Chem. 53 (2021) 234–240.
[5] Z.M. Tong, L. Huang, H.P. Liu, et al., Adv. Funct. Mater. 31 (2021) 2010455.
[6] H. Ye, D.N. Lei, L. Shen, et al., Chin. Chem. Lett. 31 (2020) 570–574.
[7] S.G. Deng, Q.H. Li, Y.H. Chen, et al., Inorg. Chem. Front. 8 (2021) 1771–1778.
[8] H.L. Wan, S.F. Liu, T. Deng, et al., ACS Energy Lett. 6 (2021) 862–868.
[9] J.H. Wu, S.F. Liu, F.D. Han, X.Y. Yao, C.S. Wang, Adv. Mater. 33 (2021) 31–48.
[10] Q. Zhang, H.L. Wan, G.Z. Liu, et al., Nano Energy 57 (2019) 771–782.
[11] B. Guan, X. Sun, Y. Zhang, et al., Chin. Chem. Lett. 32 (2021) 2249–2253.
[12] C.Y. Zhou, J. Wang, X.B. Zhu, et al., Nano Res. 14 (2021) 1541–1550.
[13] J.Y. Cui, Z.H. Li, G.R. Wang, J. Guo, M.F. Shao, J. Mater. Chem. A 8 (2020) 23738–23755.
[14] F. Wu, S.Y. Zhao, L. Chen, et al., Energy Storage Mater. 14 (2018) 383–391.
[15] W. Wang, C. Liao, K.M. Liew, et al., J. Mater. Chem. A 7 (2019) 6859–6868.
[16] S.Y. Bai, X.Z. Liu, K. Zhu, S.C. Wu, H.S. Zhou, Nat. Energy 1 (2016) 16094.
[17] X. Wang, G. Li, M. Li, et al., J. Energy Chem. 53 (2021) 234–240.
[18] C. Chen, Q.B. Jiang, H.F. Xu, et al., Nano Energy 76 (2020) 105033.
[19] P. Cheng, P.Q. Guo, K. Sun, et al., J. Membr. Sci. 619 (2021) 118780.
[20] J.F. Wang, J. Li, J. Colloid Interface Sci. 584 (2021) 354–359.
[21] Z.Y. Wang, Y.F. Dong, H.J. Li, et al., Nat. Commun. 5 (2014) 8–15.
[22] Z.B. Liu, L. Wang, W.T. Yang, Chin. Chem. Lett. 32 (2021) 2919–2922.
[23] T.Z. Hou, X. Chen, H.J. Peng, et al., Small 12 (2016) 3283–3291.
[24] K.L. Ai, Y.L. Liu, C.P. Ruan, L.H. Lu, G.Q. Lu, Adv. Mater. 25 (2013) 998–1003.
[25] Y.G. Zhang, Y. Zhao, A. Yermukhambetova, Z. Bakenov, P. Chen, J. Mater. Chem. A 1 (2013) 295–301.
[26] Q.H. Li, J. Yang, Y. Zhao, et al., New J. Chem. 44 (2020) 5965–5971.
[27] X.Y. Yao, C.Y. Zhao, J.H. Kong, et al., Chem. Commun. 50 (2014) 14597–14600.
[28] D. Zhou, L.P. Yang, L.H. Yu, et al., Nanoscale 7 (2015) 1501–1509.
[29] Z. Su, M.Q. Chen, Y.K. Pan, et al., J. Mater. Chem. A 8 (2020) 24117–24127.
[30] Y.J. Liu, M.Q. Chen, Z. Su, et al., Carbon 172 (2021) 260–271.
[31] Y. Chen, Q. Kang, P.K. Jiang, X.Y. Huang, Nano Res. 14 (2021) 2424–2431.

[32] J.S. Yeon, T.H. Park, Y.H. Ko, et al., J. Energy Chem. 55 (2021) 468–475.
[33] H.G. Jin, M.Y. Wang, J.X. Wen, et al., ACS Appl. Mater. Interfaces 13 (2021) 3899–3910.
[34] Q. Wang, H.Q. Zhao, B.Y. Li, et al., Chin. Chem. Lett. 32 (2021) 1157–1160.
[35] J. Wang, L.J. Jia, S.R. Duan, et al., Energy Storage Mater. 28 (2020) 375–382.
[36] Y. Song, X.Y. Li, C.Z. He, Chin. Chem. Lett. 32 (2021) 1106–1110.
[37] L.L. Zhang, D.B. Liu, Z. Muhammad, et al., Adv. Mater. 31 (2019) 9–20.
[38] Y.J. Zhu, Y.Z. Zuo, F. Ye, et al., Chem. Eng. J. 428 (2022) 131109.